Dynamics and control of robotic spacecrafts for the transportation of flexible elements

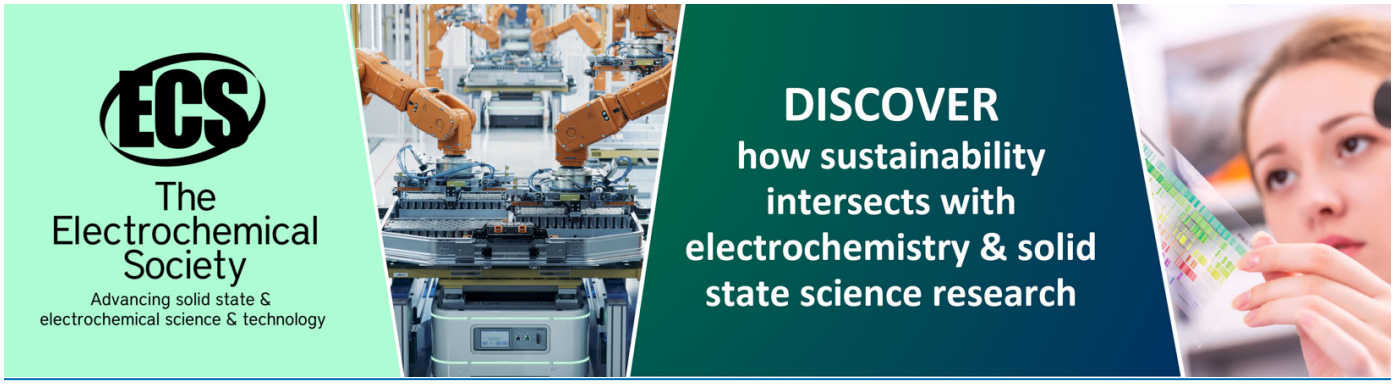

Dynamics and control of robotic spacecrafts for the transportation of flexible elements

Hao Wen, Ti Chen, Bensong Yu and Dongping Jin

State Key Laboratory of Mechanics and Control of Mechanical Structures, Nanjing University of Aeronautics and Astronautics, Nanjing 210016, China

wenhao@nuaa.edu.cn

Abstract. The technology of robotic spacecrafts has been identified as one of the most appealing solutions to the on-orbit construction of large space structures in future space missions. As a prerequisite of a successful on-orbit construction, it is needed to use small autonomous spacecrafts for the transportation of flexible elements. To this end, the paper presents an energy-based scheme to control a couple of robotic spacecrafts carrying a flexible slender structure to its desired position. The flexible structure is modelled as a long beam based on the formulation of absolute nodal coordinates to account for the geometrical nonlinearity due to large displacement. Meanwhile, the robotic spacecrafts are actuated on their rigid-body degrees of freedom and modelled as two rigid bodies attached to the flexible beam. The energy-based controller is designed using the technique of energy shaping and damping injection such that translational and rotational maneuvers can be achieved with the suppression of the flexible vibrations of the beam. Finally, numerical case studies are performed to demonstrate the proposed schemes.

1. Introduction

Future developments in space science and engineering will require ever larger space systems, such as space solar power station, large-aperture space telescopes, etc. To meet the requirements of such space missions, the space structures will be constructed too large to be launched and deployed as a whole [1, 2]. The technology of robotic spacecrafts has been identified as one of the most appealing solutions to the on-orbit construction of such large space structures. For example, in the 1990s, NASA Langley research center developed a robotic system to autonomously assemble and disassemble a space truss structure [1]. Whittaker et al. presented a conceptual investigation on the use of space robots to autonomously assemble, inspect, and maintain space solar-power facilities, and identified the main technical challenges facing the proposed concept [2]. Lillie examined the on-orbit assembling and servicing concepts for the applications of future space observatories, and proposed conceptual designs in accordance with typical mission scenarios [3]. Badawy and McInnes used super-quadrics surfaces to describe the bounding boxes for collision avoidance, and proposed a collision-free control scheme for the autonomous assembly of a large space structure [4]. Hu et al. designed a formation controller of four robots for the on-orbit construction of a large solar sail with a hub as the central body and four large booms supporting the lightweight films [5].

Although technically appealing, autonomous assembly of any large flexible space structure is quite challenging from the viewpoints of dynamics and control. One problem of great concern is that the

flexible vibrations of structural members may be easily excited by robotic operations during the assembly process and hardly damped out in space environment due to the low-damping characteristics of the flexible structures. Besides, it poses a greatly challenging output-feedback and under-actuated control problem that the actuating and sensing resources available to such space systems are quite limited. Over the past decades, the motion and vibration control problems concerning autonomous assembly of flexible space structures have gained a great attention from academic and engineering communities. For example, Katz et al. presented controller designs and ground-based experiments to demonstrate the assembly of a flexible space structures using the Self-Assembling Wireless Autonomous Reconfigurable Modules (SWARM) hardware [6]. Boning and Dubowsky proposed to use teams of space robots for transporting, manipulating and assembling large flexible space structures on orbit, and applied the linear optimal control theory to control the robots and minimize structural vibrations [7]. Chen et al. devised a compound control scheme combining an output consensus controller and a collision avoidance controller for a team of hub-beam systems, and proposed a control strategy with four steps to achieve the assembly mission of a flexible space structure and suppress the vibration of flexible elements [8].

Notably, as a prerequisite for autonomously assembling flexible space structures, it is required to use small autonomous spacecrafts for transportation of flexible elements. It is evident that the motion and vibration control of the robotic spacecrafts is essential for the success of the transportation tasks. In this paper, an energy-based scheme is proposed to control a couple of robotic spacecrafts carrying a flexible slender structure to its desired position. The flexible structure is modelled as a long beam based on the Absolute Nodal Coordinate Formulation (ANCF) so as to account for the geometrical nonlinearity due to large displacement [9, 10]. Meanwhile, the robotic spacecrafts are actuated on their rigid-body degrees of freedom and modelled as two rigid bodies attached to the flexible beam. The energy-based controller is designed using the technique of energy shaping and damping injection such that translational and rotational maneuvers can be achieved with the suppression of the flexible vibrations of the beam. Furthermore, the physical bounds of control inputs are accommodated using special saturation functions. Finally, numerical case studies are performed to demonstrate the proposed scheme.

2. Dynamics Modelling

The system of concern consists of a long slender flexible element and a couple of robotic spacecrafts, as shown in figure 1. To focus on the fundamental issues of the control problem, the attention of the paper is limited to planar motions. Besides, the effect of orbital mechanics is neglected since the time-scale of the task under consideration is much smaller than the orbital period of the system. The system motions are described using an inertial frame $O-xy$. The two robotic spacecrafts clamped to the ends of the flexible element are simplified as rigid bodies in circular shape. The centroid, radius, mass and rotational angle of the rigid body s are denoted by O_s, R_s, m_s and θ_s for $s \in \{A, B\}$, respectively.

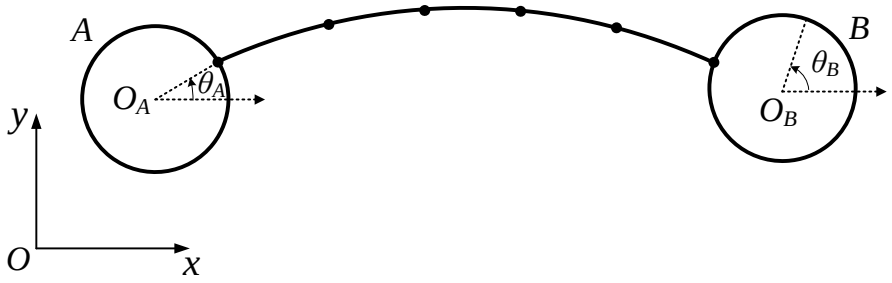

Figure 1. A couple of robotic spacecrafts carrying a flexible slender beam.

The attitude angles of the rigid bodies are measured with respect to the positive direction of the $O-x$ axis. Accordingly, the kinetic energy of the rigid body $s \in \{A, B\}$ is given by

$$T_s = \tfrac{1}{2} m_s (\dot{x}_s^2 + \dot{y}_s^2) + \tfrac{1}{2} J_s \dot{\theta}_s^2 \tag{1}$$

where the dot represents the derivative with respect to time, $(x_s, y_s)^{\mathrm{T}}$ denotes the coordinate pair of the global position vector $\boldsymbol{r}_s$ of O_s with respect to the inertial frame, $J_s = \tfrac{1}{2} m_s R_s^2$ is the moment of inertia with respect to the centroid of s. Defining the generalized coordinates $\boldsymbol{q}_s$ and the inertia matrix $\boldsymbol{M}_s$ as

$$\boldsymbol{q}_s = (x_s, y_s, \theta_s)^{\mathrm{T}}, \quad \boldsymbol{M}_s = \mathrm{diag}(m_s, m_s, J_s) \tag{2}$$

one arrives at the following dynamics equation

$$\boldsymbol{M}_s \ddot{\boldsymbol{q}}_s - \boldsymbol{Q}_s = 0 \tag{3}$$

where $\boldsymbol{Q}_s$ is the generalized force associated with $\boldsymbol{q}_s$, and ' diag ' denotes a diagonal matrix with the inputs arguments on the main diagonal.

The ANCF scheme is used to model the flexible element as a long beam of original length L such that the geometrical nonlinearity due to large displacement can be accounted for [9, 10]. The density and cross sectional shape of the beam are assumed to be uniform along its length. The cross section of the beam has a rectangular shape with wideness w_b (defined along the direction perpendicular to the $O-xy$ plane), thickness t_b, and area $A = w_b t_b$. In the ANCF method, the flexible beam are discretized into N elements equal in length to each other in the undeformed state. The nodal coordinates $\boldsymbol{e}_i$ of the ith element consist of the absolute slopes and displacements at the nodal points i and $i+1$, as shown in figure 2, that is

$$\boldsymbol{e}_i = \left(\boldsymbol{\xi}_i;\ \boldsymbol{\xi}_{i+1}\right), \quad \boldsymbol{\xi}_i = \left(x_i, y_i, \frac{\partial x_i}{\partial \eta}, \frac{\partial y_i}{\partial \eta} \right)^{\mathrm{T}}, \quad i \in 1, 2, \ldots, N \tag{4}$$

where the semicolon represents vertical concatenation of vectors, $\eta \in [0, L_e]$ is the curve coordinate of an arbitrary point p on the neutral axis of the beam element in the undeformed configuration, and $L_e = L / N$ is the original length of the element.

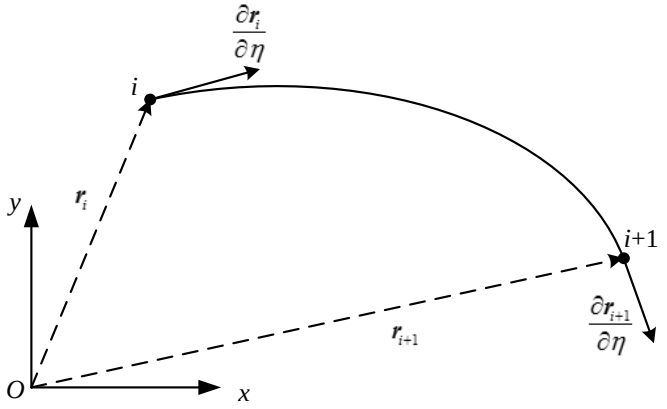

Figure 2. The ith beam element between node i and node $i+1$.

The global position $\boldsymbol{r} = (x, y)^{\mathrm{T}}$ of p can be described using a shape function matrix $\boldsymbol{S}$ and the nodal coordinates $\boldsymbol{e}_i$ as follows

$$\boldsymbol{r} = \boldsymbol{S}\boldsymbol{e}_i = [S_1\boldsymbol{I}, S_2\boldsymbol{I}, S_3\boldsymbol{I}, S_4\boldsymbol{I}]\boldsymbol{e}_i \tag{5}$$

where the interpolating functions are given by [9]

$$S_1 = 1-3\zeta^2+2\zeta^3,\ S_2 = L_e\left(\zeta-2\zeta^2+\zeta^3\right),\ S_3 = 3\zeta^2-2\zeta^3,\ S_4 = L_e\left(\zeta^3-\zeta^2\right) \tag{6}$$

and $\zeta \in [0,1]$ denotes the dimensionless coordinate defined by $\zeta = \eta / L_e$.

It follows from equation (5) that the kinetic energy of the beam element yields

$$T_{e_i} = \frac{1}{2}\int_0^{L_e} \rho A\dot{\boldsymbol{r}}^{\mathrm{T}}\dot{\boldsymbol{r}}\mathrm{d}\eta = \frac{L_e\rho_l}{2}\int_0^1 \dot{\boldsymbol{r}}^{\mathrm{T}}\dot{\boldsymbol{r}}\mathrm{d}\zeta = \frac{1}{2}\dot{\boldsymbol{e}}_i^{\mathrm{T}}\boldsymbol{M}_e\dot{\boldsymbol{e}}_i \tag{7}$$

where the element mass matrix $\boldsymbol{M}_e$ is given by

$$\boldsymbol{M}_e = \rho_l L_e\int_0^1 \boldsymbol{S}^{\mathrm{T}}\boldsymbol{S}\mathrm{d}\zeta \tag{8}$$

and ρ and ρ_l is the density and linear density of the beam in the undeformed state, respectively. It is worth noting that the ANCF scheme leads to a constant element mass matrix.

The elastic potential due to longitudinal and bending deformations can be written as

$$U_{e_i} = \frac{1}{2}\int_0^{L_e} EA\varepsilon^2\mathrm{d}\eta + \frac{1}{2}\int_0^{L_e} EI\kappa^2\mathrm{d}\eta \tag{9}$$

where E, I, ε and κ denote the modulus of elasticity, second moment of area, longitudinal strain and curvature of the beam element. The generalized elastic force $\bar{\boldsymbol{Q}}_{e_i}$ associated with the nodal coordinates $\boldsymbol{e}_i$ is given by

$$\bar{\boldsymbol{Q}}_{e_i} = \left(\frac{\partial U_{e_i}}{\partial \boldsymbol{e}_i}\right)^{\mathrm{T}} = \int_0^{L_e} EA\varepsilon\frac{\partial \varepsilon}{\partial \boldsymbol{e}_i}\mathrm{d}\eta + \int_0^{L_e} EI\kappa\frac{\partial \kappa}{\partial \boldsymbol{e}_i}\mathrm{d}\eta \tag{10}$$

Consequently, the dynamic equation of the element is derived as

$$\boldsymbol{M}_e\ddot{\boldsymbol{e}}_i - \boldsymbol{Q}_{e_i} = 0, \quad \boldsymbol{Q}_{e_i} = \tilde{\boldsymbol{Q}}_{e_i} - \bar{\boldsymbol{Q}}_{e_i} \tag{11}$$

where $\tilde{\boldsymbol{Q}}_{e_i}$ denotes the generalized external force associated with the nodal coordinates. It is worth noticing that the worst case without any internal structural damping is taken for consideration in the present work. Assembling the equations of all the N elements yields the dynamics equation of the beam $\boldsymbol{M}_\xi\ddot{\boldsymbol{\xi}} + \boldsymbol{Q}_\xi = 0$, where $\boldsymbol{\xi} = (\boldsymbol{\xi}_1; \boldsymbol{\xi}_2; \ldots; \boldsymbol{\xi}_2)$ consists of all the nodal coordinates of the beam, $\boldsymbol{M}_\xi$ denotes the total mass matrix, and $\boldsymbol{Q}_\xi$ is an assembly of all the elastic and external forces on the beam.

Up to this point, the dynamics equations of the rigid bodies and the beam are derived individually without consideration of the coupling constraints between them. Applying the method of Lagrange multiplier yields the following motion and constraint equations of the whole system [11]

$$\boldsymbol{M}\ddot{\boldsymbol{q}} + \boldsymbol{Q} + \left(\frac{\mathrm{d}\boldsymbol{\Phi}}{\mathrm{d}\boldsymbol{q}}\right)^{\mathrm{T}}\boldsymbol{\lambda} = 0, \quad \boldsymbol{\Phi} = 0 \tag{12}$$

where the generalized coordinates $\boldsymbol{q}$, the generalized forces $\boldsymbol{Q}$, the mass matrix $\boldsymbol{M}$ and the constraint function $\boldsymbol{\Phi}$ are given by

$$\boldsymbol{q} = (\boldsymbol{q}_A; \boldsymbol{\xi}; \boldsymbol{q}_B),\ \ \boldsymbol{Q} = (\boldsymbol{Q}_A; \boldsymbol{Q}_\xi; \boldsymbol{Q}_B),\ \ \boldsymbol{M} = \mathrm{diag}(\boldsymbol{M}_A, \boldsymbol{M}_\xi, \boldsymbol{M}_B),\ \ \boldsymbol{\Phi} = (\boldsymbol{\Phi}_A; \boldsymbol{\Phi}_B) \tag{13}$$

with

$$\boldsymbol{\Phi}_A=\begin{pmatrix} x_A+R_A\cos\theta_A-\xi_1 \\ y_A+R_A\sin\theta_A-\xi_2 \\ \sin\theta_A-\xi_4\Big/\sqrt{\xi_3^2+\xi_4^2} \end{pmatrix},\quad \boldsymbol{\Phi}_B=\begin{pmatrix} x_B-R_B\cos\theta_B-\xi_{4N+1} \\ y_B-R_B\sin\theta_B-\xi_{4N+2} \\ \sin\theta_B-\xi_{4N+4}\Big/\sqrt{\xi_{4N+3}^2+\xi_{4N+4}^2} \end{pmatrix} \tag{14}$$

One point of note is that the constraint function $\boldsymbol{\Phi}_s$ represents the requirements of position and orientation continuities at the connection point of the beam and the rigid body $s\in\{A, B\}$. In this work, one kind of generalized-α schemes for constrained mechanical systems is used to solve the Differential Algebraic Equations (DAEs) described by equation (12) [12].

3. Controller Design

The problem of concern is to control the two robotic spacecrafts such that the flexible structure can be carried to its desired position with the suppression of flexible vibrations. It is taken into consideration for the ease of practical implementation that the motions of the flexible beam are not directly measured and actuated on. The control actuation and state measurement of the robotic spacecrafts are available only at their rigid-body degrees of freedom. For this purpose, an energy-based controller is designed using the technique of energy shaping and damping injection. Furthermore, the physical bounds of actuators are naturally accommodated using strictly increasing saturation functions.

The proposed control law for the spacecraft $s\in\{A, B\}$ is of the following saturated form [13, 14]

$$Q_{s_j}=-\sigma(k_{s_j}^p\delta q_{s_j}+k_{s_j}^d\dot{q}_{s_j}) \tag{15}$$

where Q_{s_j} and q_{s_j} are the j th components of $\boldsymbol{Q}_s$ and $\boldsymbol{q}_s$, $\delta q_{s_j}=q_{s_j}-\overline{q}_{s_j}$ represents the error between q_{s_j} and its desired value $\overline{q}_{s_j}$, $k_{s_j}^p$ and $k_{s_j}^d$ are the non-negative position and velocity feedback gains, and σ is a strictly increasing saturation function satisfying

$$\begin{cases} \sigma_{s_j}(\alpha)=\alpha, & \text{for } |\alpha|\le\underline{\Gamma}_{s_j} \\ \left|\sigma_{s_j}(\alpha)\right|<\overline{\Gamma}_{s_j}, & \text{for } \alpha\in\mathbb{R} \end{cases} \tag{16}$$

where the given positive constants $\underline{\Gamma}_{s_j}$ and $\overline{\Gamma}_{s_j}$ satisfies $\underline{\Gamma}_{s_j}<\overline{\Gamma}_{s_j}$. Without the loss of generality, the strictly increasing saturation function is chosen as per [13]

$$\sigma_{s_j}(\alpha)=\begin{cases} -\underline{\Gamma}_{s_j}+(\overline{\Gamma}_{s_j}-\underline{\Gamma}_{s_j})\tanh\left(\dfrac{\alpha+\underline{\Gamma}_{s_j}}{\overline{\Gamma}_{s_j}-\underline{\Gamma}_{s_j}}\right) & \alpha<-\underline{\Gamma}_{s_j} \\ \alpha & -\underline{\Gamma}_{s_j}\le\alpha\le\underline{\Gamma}_{s_j} \\ \underline{\Gamma}_{s_j}+(\overline{\Gamma}_{s_j}-\underline{\Gamma}_{s_j})\tanh\left(\dfrac{\alpha-\underline{\Gamma}_{s_j}}{\overline{\Gamma}_{s_j}-\underline{\Gamma}_{s_j}}\right) & \alpha>\underline{\Gamma}_{s_j} \end{cases} \tag{17}$$

The limits of the control input can be accommodated by choosing the positive constant $\underline{\Gamma}_{s_j}$ in equation (17) to be the upper bound of the actuator force or torque. The design parameter $\underline{\Gamma}_{s_j}$ is set as $\underline{\Gamma}_{s_j}=0.9\overline{\Gamma}_{s_j}$ in this work.

It is interesting to note from equation (17) that the control input Q_{s_j} can be further decomposed into two parts as $Q_{s_j} = p_{s_j} + f_{s_j}$ with

$$p_{s_j}(\delta q_{s_j}, \dot{q}_{s_j}) = -[\sigma(k_{s_j}^p \delta q_{s_j} + k_{s_j}^d \dot{q}_{s_j}) - \sigma(k_{s_j}^d \dot{q}_{s_j})], \quad f_{s_j}(\dot{q}_{s_j}) = -\sigma(k_{s_j}^d \dot{q}_{s_j}) \tag{18}$$

In the case of the feedback gains $k_{s_j}^p$ and $k_{s_j}^d$ being positive, it follows from the increasing characteristic of the function σ that the signs of $p_{s_j}(\delta q_{s_j}, \dot{q}_{s_j})$ and $f_{s_j}(\dot{q}_{s_j})$ are opposite to those of δq_{s_j} and $\dot{q}_{s_j}$, respectively. Therefore, p_{s_j} can be viewed as a nonlinear elastic force with the responsibility of bringing the system state q_{s_j} to its desired value $\bar{q}_{s_j}$. Besides, f_{s_j} actuates as a damping force which always leads to negative power to the system. In other words, the generalized forces p_{s_j} and f_{s_j} have the effects equivalent to the addition of an artificial potential and an artificial dissipative term to the system energy. From this perspective, the design of the saturated control law naturally follows the principles of energy-based control by applying the techniques of energy shaping and damping injection [13].

4. Case Studies

The formulated dynamics model and the proposed control scheme are verified via two case studies which are the same in system parameters but different in actuating conditions. As compared to the first case, an additional toque actuator is present in the second case on the first spacecraft to exert damping force on the rotational Degree of Freedom (DOF). The feedback gains of the first case are chosen to be

$$\boldsymbol{k}^p\big|_{\text{case1}} = (0.3, 0.3, 0.0, 0.3, 0.3, 0.0)^{\mathrm{T}}, \quad \boldsymbol{k}^d\big|_{\text{case1}} = (3, 3, 0, 3, 3, 0)^{\mathrm{T}} \tag{19}$$

with the gain vectors defined by

$$\boldsymbol{k}^p = (k_{A_1}^p, k_{A_2}^p, k_{A_3}^p, k_{B_1}^p, k_{B_2}^p, k_{B_3}^p)^{\mathrm{T}}, \quad \boldsymbol{k}^d = (k_{A_1}^d, k_{A_2}^d, k_{A_3}^d, k_{B_1}^d, k_{B_2}^d, k_{B_3}^d)^{\mathrm{T}} \tag{20}$$

The feedback gains of the second case are chosen to be

$$\boldsymbol{k}^p\big|_{\text{case2}} = \boldsymbol{k}^p\big|_{\text{case1}}, \quad \boldsymbol{k}^d\big|_{\text{case2}} = (3, 3, 1, 3, 3, 0)^{\mathrm{T}} \tag{21}$$

The upper bounds of control force and toque are set to be $0.5\ \mathrm{N}$ and $0.1\ \mathrm{Nm}$, respectively.

In equations (19) and (21), it is implied by setting $k_{s_j}^p$ (or $k_{s_j}^d$) to zero on a specific DOF that no artificial elastic force (or damping force) is available on the DOF. Besides, the velocity gains are chosen to be relatively large so as to reduce the overshoots of system responses.

The spacecrafts are initially static in the following states

$$q_A\big|_{t=0} = (0, 0, 0)^{\mathrm{T}}, \quad q_B\big|_{t=0} = (R_A + R_B + L, 0, 0)^{\mathrm{T}} \tag{22}$$

and their desired states are

$$\bar{q}_A = (-5, 0, \tfrac{1}{2}\pi)^{\mathrm{T}}, \quad \bar{q}_B = (-5, R_A + R_B + L, \tfrac{1}{2}\pi)^{\mathrm{T}} \tag{23}$$

where the lengths and angles are given in meters and radians, respectively. The flexible beam is initially static in the undeformed state and aligned with the connecting line between the centroids of the spacecrafts. The ANCF model of the beam consists of four elements equal in length and five nodal points. The physical parameters of the spacecrafts are taken to be $R_s = 0.2\ \mathrm{m}$ and $m_s = 10\ \mathrm{kg}$ for $s \in \{A, B\}$, and the flexible beam has the following parameters

$$t_b = 0.002 \text{ m},\ w_b = 0.05 \text{ m},\ L = 5 \text{ m},\ E = 69 \text{ GPa},\ \rho = 2.7\times10^3 \text{ kg/m}^3 \quad (24)$$

Both the case studies are performed via numerical integrations for a period of 60 seconds. The spectral radius at infinity and step-size of the generalized-α scheme for numerical integration are chosen to be $\rho_\infty = 0.8$ and $h = 0.01\,\text{s}$. The time histories of the control forces on the two spacecrafts in the first case are shown in figure 3 where u_{Ax}, u_{Ay}, u_{Bx} and u_{By} are more intuitive notions of Q_{A_1}, Q_{A_2}, Q_{B_1} and Q_{B_2}, respectively. It is noted from figure 3 that the force inputs as per the proposed saturated control law doesn't violate the prescribed bounds and finally approach to zero as expected.

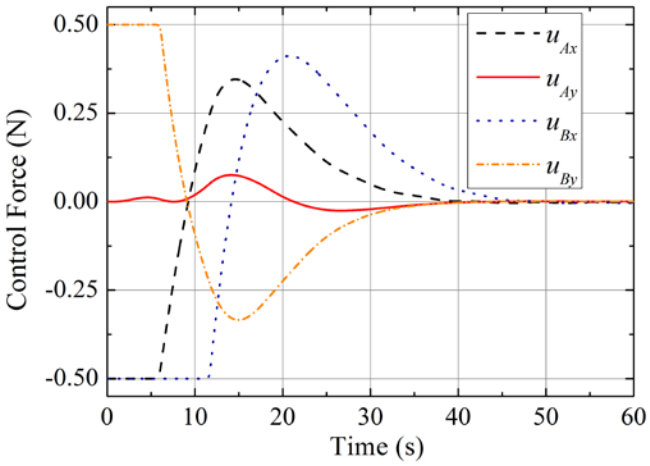

Figure 3. Time histories of the control forces in the first case

Figure 4 depicts the position responses of the two spacecrafts during the transportation task in the first case. As shown in figure 4, the proposed control law achieves quite smooth position profiles which almost exactly reach their desired values at the end of the simulation.

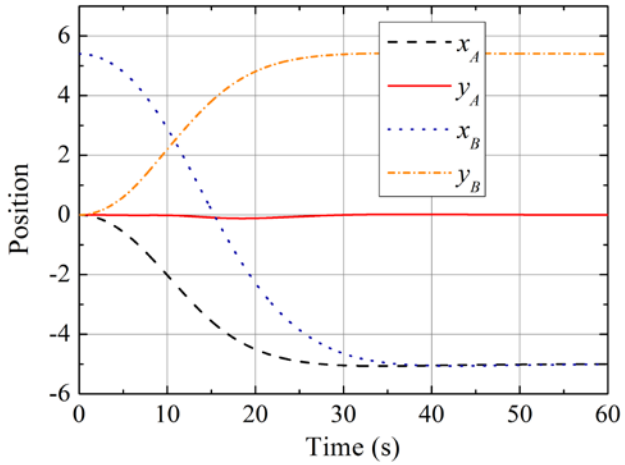

Figure 4. Time histories of the positions of the spacecrafts in the first case

The time histories of the attitude angles of the spacecrafts in the first case are shown in figure 5. It can be found from figure 5 that the attitude angles of the spacecrafts gradually converge to their desired values with small fluctuations due to the absence of torque actuation on the rotational DOF.

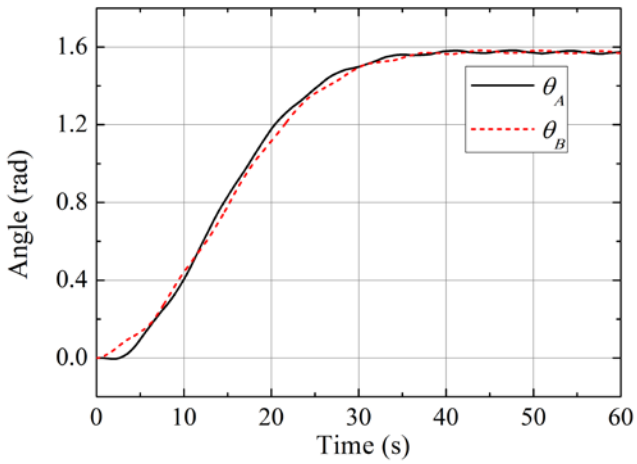

Figure 5. Time histories of the attitude angles of the spacecrafts in the first case

Figure 6 gives the time histories of the attitude angles of the spacecrafts in the second case. As compared to the first case, the addition of torque actuation on the rotation DOF of the first spacecraft leads to much smoother attitude responses. It is also shown in figure 7 that the torque input on the first spacecraft is always within the prescribed bounds. The time histories of the control inputs and spacecraft positions in the second case are not shown since they are similar in shape and amplitude to those of the first case.

5. Conclusions

The paper presents an investigation on the dynamics and control problem of using robotic spacecrafts to carry a slender flexible structure to its desired position. The flexible structure is modelled as a long beam based on the theory of ANCF which accounts by nature for the geometrical nonlinearity due to large displacement. An energy-based control law is developed to address the greatly challenging output-feedback and under-actuated control problem with the practical requirements that actuation and measurement are only available on the rigid-body DOFs of the spacecrafts. The proposed control law in the form of saturation functions naturally accommodates the physical bounds of control inputs. The proposed control scheme are demonstrated via two case studies different in actuating conditions. The results of the simulations indicate that the desired states of the transportation task can be successfully achieved using the proposed control scheme. Besides, the addition of torque actuation on the rotational DOF is beneficial to the suppression of the transient angular fluctuations of the spacecrafts.

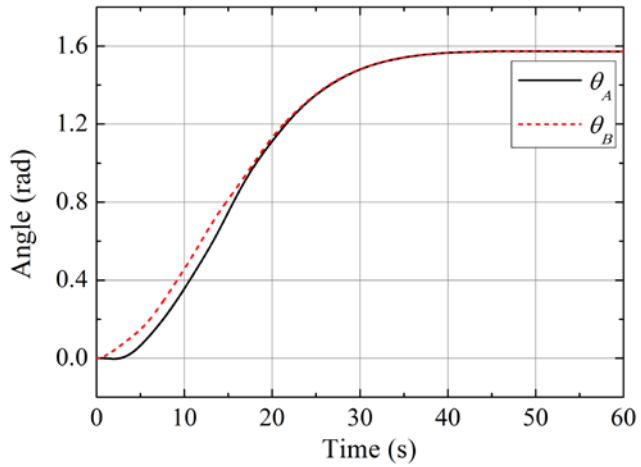

Figure 6. Time histories of the attitude angles of the spacecrafts in the second case

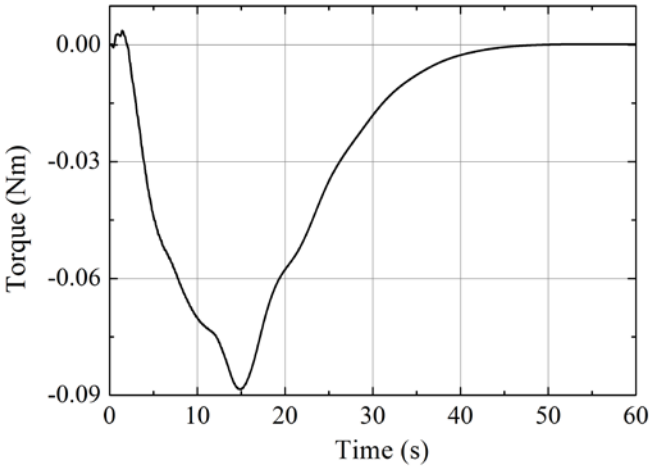

Figure 7. Time history of the control torque on the first spacecraft in the second case

Acknowledgements
This work was supported in part by the National Natural Science Foundation of China under Grant 11372130, in part by the Research Fund of State Key Laboratory of Mechanics and Control of Mechanical Structures (0113Y01), and in part by the Foundation for the Author of National Excellent Doctoral Dissertation of China under Grant 201233.

References

[1] Doggett W 2002 Robotic assembly of truss structures for space systems and future research plans. In: *IEEE Aerospace Conference*, (Big Sky, MT, United states: IEEE Computer Society)
[2] Whittaker W, Staritz P, Ambrose R, Kennedy B, Fredrickson S, Parrish J and Urmson C 2001 Robotic assembly of space solar-power facilities *Journal of Aerospace Engineering* **14** 59-64
[3] Lillie C F 2006 On-orbit assembly and servicing for future space observatories. In: *Space 2006 Conference*, (San Jose, CA, United states: American Institute of Aeronautics and Astronautics Inc.)
[4] Badawy A and McInnes C R 2008 On-orbit assembly using superquadric potential fields *J. Guid. Control Dyn.* **31** 30-43
[5] Hu Q, Zhang Y, Zhang J and Hu H 2016 Formation control of multi-robots for on-orbit assembly of large solar sails *Acta Astronaut.* **123** 446-54
[6] Katz J G, Mohan S and Miller D W 2010 On-orbit assembly of flexible space structures with SWARM. In: *AIAA Infotech at Aerospace 2010,* (Atlanta, GA, United states: American Institute of Aeronautics and Astronautics Inc.)
[7] Boning P and Dubowsky S 2010 Coordinated control of space robot teams for the on-orbit construction of large flexible space structures *Advanced Robotics* **24** 303-23
[8] Chen T, Wen H, Hu H and Jin D 2016 Output consensus and collision avoidance of a team of flexible spacecraft for on-orbit autonomous assembly *Acta Astronaut.* **121** 271-81
[9] Berzeri M and Shabana A A 2000 Development of simple models for the elastic forces in the absolute nodal co-ordinate formulation *J. Sound Vib.* **235** 539-65
[10] Shabana A A 2005 *Dynamics of Multibody Systems* (Cambridge ; New York: Cambridge University Press)
[11] Taketiara S, Terumichi Y, Nohmi M, Sogabe K and Suda Y 2005 Numerical and experimental approaches on the motion of a tethered system with large deformation, rotation and translation. In: *ASME International Design Engineering Technical Conferences and Computers and Information in Engineering Conference,* (Long Beach, CA, United states: American Society of Mechanical Engineers)

[12] Arnold M and Bruls O 2007 Convergence of the generalized- scheme for constrained mechanical systems *Multibody Sys.Dyn.* **18** 185-202
[13] Zavala-Rio A and Santibanez V 2007 A natural saturating extension of the PD-with-desired-gravity-compensation control law for robot manipulators with bounded inputs *IEEE Trans. Rob.* **23** 386-91
[14] Wen H, Zhu Z H, Jin D and Hu H 2016 Space tether deployment control with explicit tension constraint and saturation function *J. Guid. Control Dyn.* **39** 915-20